J. Fluid Mech. (1980), *vol.* 97, *part* 3, *pp.* 417–434
Printed in Great Britain

Steady flow in rapidly rotating variable-area rectangular ducts. Part 3. Inertial perturbations for small divergences

By J. S. WALKER

Department of Theoretical and Applied Mechanics,
University of Illinois, Urbana

AND A. M. EL-CONSUL

Department of Mathematics,
University of Al-Fateh, Tripoli, Libya

(Received 2 March 1979)

This paper is part of a series treating the flow in a variable-area, rectangular duct which is rotating about an axis that is perpendicular to the duct's centre-line and parallel to one pair of walls (sides). The speed of rotation is assumed to be sufficiently large that viscous effects are confined to boundary layers and free shear layers and that inertial effects are much smaller than viscous effects everywhere. Earlier papers present inertialess solutions for a prototype with parallel sides everywhere, parallel top and bottom upstream of a cross-section, and straight, symmetrically diverging top and bottom downstream of the same cross-section. The present paper presents inertial perturbations to the inertialess solutions for the prototype when the slope of the diverging top and bottom is small. This paper begins to bridge the gap between papers treating inertialess flows in ducts with arbitrary geometries and papers treating flows with significant inertial effects in ducts with restricted geometries.

1. Introduction

Flow in a duct which is rotating about an axis perpendicular to the duct's centre-line is of interest because of its relationship to fluid motions in the atmosphere and the oceans, as well as to the flows inside turbomachinery impellers. A number of papers treat such a flow under the assumption that both the Rossby number R and the Ekman number E are small, so that the flow is inertialess and inviscid except in boundary layers and free shear layers. The solutions for the inertialess, inviscid core regions are determined by matching solutions in adjacent boundary and free shear layers, so that core solutions depend indirectly on inertial and viscous effects. The relative role of inertial and viscous effects in the boundary and free shear layers depends on the relationship between R, E and the duct's geometry.

The literature is divided into two groups of papers. One group assumes that the flow is inertialess everywhere, determines solutions for the viscous boundary and free shear layers and for the inviscid cores, and introduces these solutions into the inertia terms in the momentum equation in order to find the largest inertia term in any core or layer. For this inertia term to be negligible compared to the other terms in the momentum equation, as assumed at the beginning, a small-inertia restriction

0022-1120/80/4412-8590 $02.00

must be satisfied. This restriction takes the form $R \ll cE^j$, where the factor c and the exponent j depend upon the duct's geometry. As long as $cE^j \ll 1$, this restriction is more severe than the original assumption that $R \ll 1$.

Jacobs (1964) treats the inertialess flow between two infinite, parallel walls which are perpendicular to the axis of rotation. On one wall there is a three-dimensional bump, e.g. a hemisphere, with height $h = O(1)$, compared to the distance between the walls. The fluid is stagnant in the cylinder above the bump and parallel to the axis of rotation, i.e. a Taylor column, while there is two-dimensional irrotational flow around the stagnant column. The small-inertia restriction for this flow is $R \ll E^{\frac{1}{2}}$. Walls which are parallel to the axis of rotation and to the velocity far from the bump, i.e. sides, can be added to form a constant-area rectangular duct with a bump on its top or bottom. The basic characteristics of the flow and the small-inertia restriction are unchanged.

Foster (1975) treats the inertialess flow past a similar bump on one of two infinite, parallel walls, but varies the dimension of the bump perpendicular to the axis of rotation and to the flow direction. As the width of the bump becomes very large, the flow goes over the bump, rather than around the stagnant column above it. The small-inertia restriction becomes more severe as the bump width increases, finally becoming $R \ll E^{\frac{3}{4}}$ for flow over a very long ridge perpendicular to the flow direction. Sides can be added to form a constant-area rectangular duct, where now the flow is over the bump, and the restriction is $R \ll E^{\frac{3}{4}}$, when the bump spans the duct from side to side.

A second group of papers treats flow in which inertial and viscous effects are comparable, but with restrictions on the geometry. The flows are confined by either two infinite, parallel walls, perpendicular to the axis of rotation, or by a constant-area, rectangular duct with one pair of walls (sides) parallel to the axis of rotation. There are two, symmetric bumps or ridges on the walls perpendicular to the axis of rotation (top and bottom), but the height of the bumps or ridges is small, $h = \kappa E^{\frac{1}{2}}$, while $R = \lambda E^{\frac{1}{2}}$, where κ and λ are $O(1)$ parameters.

Boyer (1971) treats the two-dimensional flow between infinite walls with ridges of constant cross-section perpendicular to the flow direction. Huppert & Stern (1974) add sides to Boyer's geometry, where the addition of sides now makes a fundamental difference. Vaziri & Boyer (1971) treat the three-dimensional flow past bumps either on infinite walls or on the top and bottom of a rectangular duct which is wider than the bumps.

The present paper is the beginning of a bridge between the papers on inertialess flows with arbitrary geometry and the papers on inertial–viscous flows with restricted geometry. It is part of a series of papers treating flows in variable-area rectangular ducts which are rotating about axes perpendicular to their centre-lines and parallel to one pair of walls (sides). These flows are closely related to the flows past constant cross-section ridges which span constant-area, rectangular ducts. Solutions are presented for a prototype with parallel sides for all x, with parallel top and bottom upstream ($x < 0$) and with straight, symmetrically diverging top and bottom downstream ($x > 0$), where the x axis coincides with the duct's centre-line (see figure 1). Part 1 (Walker 1975) presents inertialess solutions for $b = O(1)$, where b is the slope of the diverging top and bottom. Part 1 also presents a method of constructing an inertialess solution for any duct with symmetrically diverging or converging top and bottom

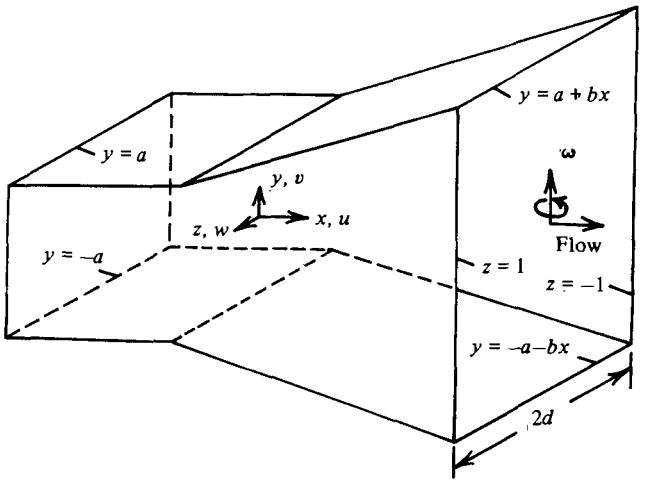

FIGURE 1. The duct.

All regions and stages: $\phi = \partial/\partial y = 1, \quad v = bu$

Stage 1: $E^{\frac{1}{4}} \ll b \ll 1, \quad \delta_s = E^{\frac{1}{3}}b^{-\frac{1}{3}}$
Stage 2: $b = \alpha E^{\frac{1}{4}}, \quad \delta_s = E^{\frac{1}{4}}$
Stage 3: $E^{\frac{1}{2}} \ll b \ll E^{\frac{1}{4}}, \quad \delta_s = E^{\frac{1}{2}}b^{-1}$
Stages 1, 2, 3: $\delta_f = E^{\frac{1}{2}}b^{-\frac{1}{2}}$
Free shear layer: $u = \partial/\partial z = 1, \quad w = \partial/\partial x = \delta_f^{-1}$
Intersection region: $u = \partial/\partial z = \delta_s^{-1}, \quad w = \partial/\partial x = \delta_f^{-1}$
Side layer: $u = \partial/\partial z = \delta_s^{-1}, \quad w = \partial/\partial x = b$
Stage 4: $b = \mu E^{\frac{1}{2}}, \quad u = \partial/\partial z = 1$
Near core: $w = \partial/\partial x = 1$, far core: $w = \partial/\partial x = b$

TABLE 1. Orders of magnitude of derivatives and inertialess variables in each flow-carrying region for each stage (see figure 2).

from the solutions for the prototype and discusses the extension of the analysis to ducts with symmetrically diverging or converging sides. Part 2 (Calderon & Walker 1977) presents inertialess solutions for the prototype for small b. There are four stages between $b = 1$ and $b = 0$, and the values of b for each stage are given in table 1 here. The solutions for the free shear layer at $x = 0$ which are presented in part 2 are wrong, and the correct inertialess solutions for the free shear layer are presented in § 3 of this paper.

The present paper presents the inertial perturbations to the inertialess solutions for the prototype with small b. The small-slope ducts were chosen for two reasons. Analytical solutions are possible for small b, while numerical solutions are required for $b = O(1)$, making the construction and interpretation of inertial perturbations for $b = O(1)$ much more complex. In addition, the effect of a small slope is closely related to the β effect on fluid motions in the atmosphere and the oceans (Hseuh & Legeckis 1973), so that the small-slope ducts are important in themselves.

The inertialess solutions and the inertial perturbations are the first and second terms, respectively, in asymptotic expansions for small inertial effects, i.e. for

$\epsilon = R/cE^j \ll 1$. Therefore, the small-inertia restriction for each stage must still be satisfied, but now we have the first inertial correction to each inertialess solution.

The inertial perturbations are useful in several ways. First, when inertial effects are, in reality, small, but not negligible, e.g. $\epsilon = 0{\cdot}1$, then calculations based on the first two terms of the small-inertia asymptotic expansions are more accurate than those based on the inertialess solutions alone. Second, finding the inertial perturbations defines the small-inertia restriction for different values of b, namely

$$\begin{aligned}
&R \ll E^{\frac{11}{12}} && \text{for} \quad b = O(1);\\
&R \ll E^{\frac{11}{12}} b^{-\frac{1}{6}} && \text{for} \quad E^{\frac{1}{4}} \ll b \ll 1;\\
&R \ll E^{\frac{7}{8}} && \text{for} \quad b = \alpha E^{\frac{1}{4}};\\
&R \ll E^{\frac{5}{6}} b^{-\frac{2}{3}} && \text{for} \quad E^{\frac{1}{2}} \ll b \ll E^{\frac{1}{4}};\\
&R \ll E^{\frac{1}{2}} && \text{for} \quad b = \mu E^{\frac{1}{2}}.
\end{aligned}$$

The small-inertia restrictions given in parts 1 and 2 are wrong; it takes more than a casual look at the inertialess solutions to determine the correct small-inertia restrictions. Third, the inertial perturbations answer the question 'Do small inertial effects somehow accumulate over large duct lengths so that they are no longer negligible far downstream?'; the answer is no. Fourth, the inertial perturbations indicate what the inertial effects are in each subregion of the flow for each stage and the relative size of the inertial effects in different subregions. As we consider the possibility of relaxing the small-inertia restrictions, we know where the inertial effects first become comparable to viscous effects, while the inertial perturbation in this subregion indicates qualitatively how solutions for comparable viscous and inertial effects will differ from inertialess solutions. At present, the solutions for stage 4, with $b = \mu E^{\frac{1}{2}}$ and $R \ll E^{\frac{1}{2}}$, represent the closest link with the inertial–viscous solutions for restricted geometry presented by Boyer (1971) and by Huppert & Stern (1974).

2. General considerations

The flow considered here is incompressible and steady relative to a Cartesian coordinate system rotating at a constant angular velocity $\boldsymbol{\omega} = \omega\hat{\mathbf{y}}$ with respect to some inertial system. The dimensionless governing equations are

$$\nabla.\mathbf{v} = 0, \quad R(\mathbf{v}.\nabla)\,\mathbf{v} = -\nabla\phi - \hat{\mathbf{y}} \times \mathbf{v} + E\nabla^2\mathbf{v}, \tag{1a, b}$$

where the reduced pressure ϕ includes the potential functions for the centrifugal and gravitational forces, as well as the pressure (Greenspan 1968, p. 6). Here $\hat{\mathbf{y}}$ is a unit vector in the y direction, $\mathbf{v}$ is the velocity, $R = U/2\omega d$ is the Rossby number, $E = \nu/2\omega d^2$ is the Ekman number, U is a characteristic velocity, d is a characteristic length and ν is the kinematic viscosity. The scalar components of equation (1b) are

$$\partial\phi/\partial y = E\nabla^2 v - R(\mathbf{v}.\nabla)\,v, \tag{2a}$$

$$u = \partial\phi/\partial z - E\nabla^2 w + R(\mathbf{v}.\nabla)\,w, \tag{2b}$$

$$w = -\partial\phi/\partial x + E\nabla^2 u - R(\mathbf{v}.\nabla)\,u, \tag{2c}$$

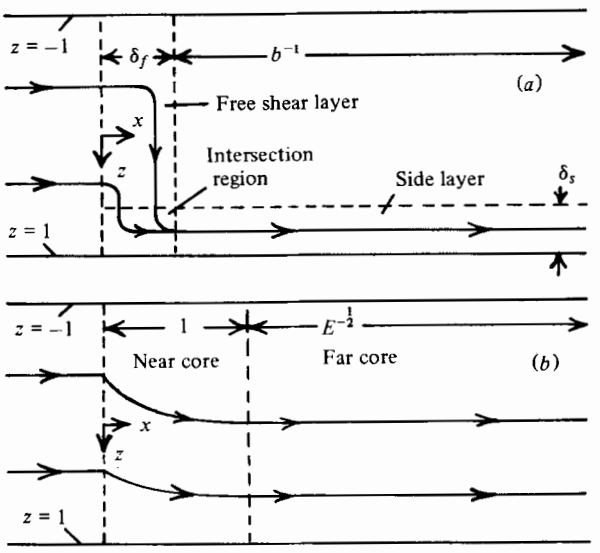

FIGURE 2. Horizontal sections at $y = 0$ showing the regions which carry the $O(1)$ flow and a sketch of streamlines for (*a*) $1 \gg b \gg E^{\frac{1}{2}}$ (stages 1, 2 and 3) and (*b*) $b = \mu E^{\frac{1}{2}}$ (stage 4).

while equations (1*a*), (2*b*, *c*) give

$$\partial v/\partial y = E\nabla^2(\partial w/\partial x - \partial u/\partial z) + R\,\partial(\mathbf{v}.\nabla)\,u/\partial z - R\,\partial(\mathbf{v}.\nabla)\,w/\partial x,$$

where u, v and w are the x, y and z components of $\mathbf{v}$, respectively.

The flow is confined by a pair of semi-infinite rectangular ducts joined at $x = 0$ to give a prototype with parallel sides at $z = \pm 1$ for all x, parallel top and bottom at $y = \pm a$ upstream ($x < 0$) and straight, diverging top and bottom at $y = \pm(a + bx)$ downstream ($x > 0$), where half the distance between the sides is chosen for d (see figure 1). For small divergences ($b \ll 1$), the flow in the upstream, constant-area duct is fully developed, neglecting an $O(b)$ perturbation (Calderon & Walker 1977). Here we treat the flow in the downstream, variable-area duct, while the solution for fully developed flow is obtained by setting $b = 0$ in the solution for the fourth stage here. The average velocity at $x = 0$ is chosen for U, so that the dimensionless solution must satisfy the total-flow condition

$$\int_{-1}^{1}\int_{-(a+bx)}^{(a+bx)} u\,dy\,dz = 4a. \tag{3}$$

The boundary conditions are

$$\mathbf{v} = 0 \quad \text{at} \quad y = \pm(a+bx), \quad z = \pm 1. \tag{4a, b}$$

We assume that $E \ll 1$ and that R is sufficiently small that variables can be written as asymptotic expansions for small inertial effects, such as $\phi = \phi_0 + \epsilon\phi_1 + O(\epsilon^2)$, where ϕ_0 and ϕ_1 are the inertialess solution and first inertial perturbation, respectively, while ϵ is a small parameter which equals R times some combination of E and b. The interior of the downstream duct can be divided into subregions, where this division depends on b. There are four stages between $b = 1$ and $b = 0$, and values of b for each stage are given in table 1. For the first three stages, the flow from the up-

stream duct enters a free shear layer which spans the duct at $x = 0$ and which has a thickness δ_f (see figure 2). The flow is carried by a large velocity to the side at $z = 1$, where the flow turns inside an intersection region and enters the side layer of thickness δ_s adjacent to the side at $z = 1$. The fluid outside these regions in the downstream duct is essentially stagnant. The solutions for the side layer and intersection region, as well as the expression for δ_s, are different for each of the first three stages (see table 1). For stage 1, the Ekman pumping is not important in this layer and region, while the y variation of v is important; for stage 3, the reverse is true; for stage 2, both are important. For stage 4, the flow enters a near-core region at $z = 0$ and moves toward the side at $z = 1$; beyond the near core is a far core in which the flow evolves slowly with $\partial/\partial x = E^{\frac{1}{2}}$. The orders of magnitude of the partial derivatives and the inertialess variables for each stage are given in table 1.

Each of the regions shown in figure 2 is separated from the top and bottom at $y = \pm(a+bx)$ by Ekman layers with $O(E^{\frac{1}{2}})$ thickness. The well-known, inertialess solution for the Ekman layers satisfies the boundary conditions (4*a*) and matches the solution in the adjacent region, provided the latter satisfies the Ekman conditions at $y = \pm(a+bx)$. It turns out that $O(E^{\frac{1}{2}}b\nabla\mathbf{v})$ and $O(E^{\frac{1}{2}}\partial v/\partial y)$ terms are negligible here, so that the Ekman conditions reduce to

$$bu \mp v = (E/2)^{\frac{1}{2}}(\partial u/\partial z - \partial w/\partial x) \quad \text{at} \quad y = \pm(a+bx) \tag{5}$$

(Greenspan 1968, p. 92). The Ekman conditions (5) hold for the inertialess solutions in all subregions and for the inertial perturbations in those subregions for which the perturbations are much larger than those in the adjacent Ekman layers. It turns out that the inertial perturbations in certain $E^{\frac{1}{4}}$ thickness side layers and in the adjacent Ekman layers are comparable, and a new Ekman condition must be derived for the inertial perturbations in these side layers (see § 4).

The intersection region, side layer and cores are separated from the side by $E^{\frac{1}{3}}$-thickness viscous layers. These layers satisfy the boundary conditions (4*b*) and match the variables in the adjacent region, as long as the latter satisfy the conditions

$$u = w = 0 \quad \text{at} \quad z = \pm 1, \tag{6}$$

and v in the adjacent region is an odd function of y (Howard 1969). For stages 3 and 4, the side layer, intersection region and cores are separated from the $E^{\frac{1}{3}}$ viscous layers by $E^{\frac{1}{4}}$-thickness viscous layers. These layers satisfy the conditions (6) and match the variables in the adjacent regions, but make no contribution to the $O(1)$ or $O(\epsilon)$ total flow. These viscous layers accept $O(1)$ or $O(\epsilon)$ flow from the side layer or far core, but this flow is returned to these regions, via the Ekman layers, at the same cross-section that it enters the viscous layers and never contributes to the flow along the duct (Calderon & Walker 1977). Inertial perturbations in the $E^{\frac{1}{3}}$ and $E^{\frac{1}{4}}$ viscous layers adjacent to the sides are not considered here, unless they are larger than the inertial perturbations in adjacent flow-carrying regions.

Our objective is to determine the inertial perturbation in each flow-carrying subregion for each stage. For a given stage, the order of magnitude of the inertial terms is different in different subregions, raising the possibility that the largest inertial perturbation in a subregion arises from matching that in an adjacent subregion, rather than from its own inertial terms. However, it turns out that, whenever one subregion's perturbation is larger than its neighbour's, it decays exponentially as we

go from one subregion to the other. Therefore, the largest inertial perturbation in each region arises from inertial terms in its governing equations, and ϵ is different for each subregion and each stage. The present small-inertia expansion scheme holds only if the largest ϵ for any subregion for a given stage is small, and this gives rise to the small-inertia restriction on R for each stage.

For a given subregion and a given stage, the x and z co-ordinates in equations (2) and (5) are rescaled according to the orders of magnitude given for $\partial/\partial x$ and $\partial/\partial z$ in table 1, so that the partial derivatives with respect to the rescaled co-ordinates are $O(1)$. Next, two-term expansions are introduced for each variable, where the order of magnitude of the inertialess term is given in table 1, and the inertial perturbation is the same, times ϵ. For example, in the intersection region for stage 1,

$$u = E^{-\frac{1}{3}}b^{\frac{1}{3}}(u_0+\epsilon u_1), \quad v = E^{-\frac{1}{3}}b^{\frac{1}{3}}(v_0+\epsilon v_1), \quad w = E^{-\frac{1}{3}}b^{\frac{1}{3}}(w_0+\epsilon w_1) \quad \text{and} \quad \phi = \phi_0+\epsilon\phi_1.$$

Setting $\epsilon = R = 0$, equations (2) become the equations governing the inertialess variables u_0, v_0, w_0 and ϕ_0, where most, if not all, of the viscous terms are negligible. With the inertialess variables in the terms with R and the inertial perturbations in the other terms, equations (2) determine ϵ and become the equations governing the inertial perturbations u_1, v_1, w_1 and ϕ_1. These equations are identical to the inertialess equations with inhomogeneous terms from $(\mathbf{v}_0.\nabla)\,\mathbf{v}_0$ added. In every case, $\phi_0, \phi_1, u_0, u_1, w_0$ and w_1 are independent of y, while v_0 and v_1 are at most linear functions of y. The conditions (5) bceome equations governing ϕ_0 and ϕ_1, and the other variables are given by derivatives of ϕ_0 and ϕ_1. The condition (3) indicates that the total flow in the inertialess solution is $4a$, while that in the inertial perturbation is zero. Calderon & Walker (1977) present inertialess solutions for the side layer, near core and far core. Here, we present inertialess solutions for the free shear layer and intersection region, as well as inertial perturbations for all flow-carrying regions.

3. Free shear layer and intersection region

Calderon & Walker (1977) present inertialess solutions for an $E^{\frac{1}{4}}$-thickness free shear layer and a corresponding intersection region for the first three stages, but it turns out that this layer and region do not occur for $b \ll 1$. Their layer consists of two semi-infinite, $E^{\frac{1}{4}}$ layers on either side of $x = 0$, with an infinite $E^{\frac{1}{3}}$ layer between them. The velocities u and w are continuous across the $E^{\frac{1}{3}}$ layer, but v is not. The $E^{\frac{1}{3}}$ layer which can accommodate this jump in v is driven by singularities at $y = \pm a$, $x = 0$. These singularities are the $E^{\frac{1}{2}} \times E^{\frac{1}{2}}$ intersections of the upstream Ekman layers at $y = \pm a$ and the downstream Ekman layers at $y = \pm (a+bx)$. For $b = O(1)$, the intersecting Ekman layers have different $O(E^{\frac{1}{4}})$ volume fluxes in the x direction, and this difference emerges into the $E^{\frac{1}{3}}$ layer at the Ekman layer as a source or sink of fluid at these points (Walker 1975). However, for $b \ll 1$, the difference in the volume fluxes in the Ekman layers is much smaller, so that the strength of the singularities is too small to drive the $E^{\frac{1}{3}}$ layer needed to accommodate the discontinuity in v in the two $E^{\frac{1}{4}}$ layers. Calderon & Walker (1977) did not treat the $E^{\frac{1}{3}}$ layer or the Ekman-layer intersections, and thus missed the error in their solution. They also failed to recognize that another, less severe type of free shear layer and accompanying intersection region, with $E^{\frac{1}{4}}b^{-\frac{1}{2}}$ thickness, is possible. Finally, they did not recognize the physically unacceptable characteristic of their solution that, for the first three stages,

their layer had $E^{\frac{1}{4}}$ thickness; then, for stage 4, it suddenly changed to $O(1)$ dimension to become the near core. In the present solution, the free shear layer evolves smoothly from $E^{\frac{1}{4}}$ thickness for $b = O(1)$, through the first three stages, to the $O(1)$ dimension of the near core for stage 4.

The solution for the free shear layer is the same for stages 1, 2, 3. Equation (2) gives

$$u_i = \partial\phi_i/\partial z, \quad w_i = -\partial\phi_i/\partial\xi, \quad v_i = -yA_i, \tag{7a, b, c}$$

where $i = 0$ or 1;

$$\xi = E^{-\frac{1}{4}}b^{\frac{1}{4}}x, \quad \epsilon = RE^{-\frac{3}{4}}b^{\frac{1}{4}},$$

$$A_0 = 0, \quad A_1 = \partial(u_0\,\partial w_0/\partial\xi + w_0\,\partial w_0/\partial z)/\partial\xi.$$

The boundary conditions (5) now give

$$2^{-\frac{1}{2}}\partial^2\phi_i/\partial\xi^2 - \partial\phi_i/\partial z = aA_i.$$

The boundary conditions

$$\phi_0 = z, \quad \phi_1 = 0 \quad \text{at} \quad \xi = 0,$$

$$\phi_0 = -1, \quad \phi_1 = 0 \quad \text{at} \quad z = -1,$$

$$\phi_0 \to -1, \quad \phi_1 \to 0 \quad \text{as} \quad \xi \to \infty,$$

come from matching the upstream core, from the condition (6) at $z = -1$, and from matching the stagnant downstream core, respectively.

Since the boundary value problems governing ϕ_i are simply the heat equation with appropriate boundary conditions, solutions can be obtained from well-known solutions. The problem governing ϕ_0 is the same as one solved by Roberts (1967, p. 189), so that

$$\phi_0 = -1 + (1+z)\,[(1+2q^2)\,B_1 - 2qB_2],$$

where

$$q = 2^{-\frac{3}{4}}\xi(1+z)^{-\frac{1}{2}}, \quad B_1 = \operatorname{erfc}(q), \quad B_2 = \pi^{-\frac{1}{2}}\exp(-q^2).$$

Equations (7*a*, *b*) now give u_0 and w_0, which, through A_1, give the inhomogeneous term in the equation governing ϕ_1. A particular solution is obtained by combining elementary solutions until the inhomogeneous term is taken care of, and then a homogeneous solution is found which cancels any non-zero values of the particular solution at $\xi = 0$, $z = -1$ and $\xi \to \infty$. The result is

$$\phi_1 = 2^{-\frac{1}{4}}a(1+z)^{\frac{1}{2}}\,[qB_1 - B_2 + 2q(B_2^2 - B_1^2) + (1-2q^2)\,B_1B_2].$$

The inertialess velocities and their inertial perturbations are now given by equations (7). The largest velocities are w_i, with w_0 carrying the total flow to the intersection region. The quantities $(1+z)^{-\frac{1}{2}}w_0$ and $2a^{-1}w_1$ depend only on q, and these universal-profile functions are plotted in figure 3. For $0 < q < 0{\cdot}35$, w_1 augments the inertialess flow, while, for $q > 0{\cdot}35$, w_1 decreases the inertialess velocity.

The solution for the intersection region is different for each stage. For stage 1, equation (2) gives equation (7*b*) and

$$u_i = \partial\phi_i/\partial\zeta, \quad v_i = -y\,\partial^4\phi_i/\partial\zeta^4 + yC_i, \tag{8a, b}$$

where

$$\zeta = E^{-\frac{1}{3}}b^{\frac{1}{3}}(z-1), \quad \epsilon = RE^{-\frac{11}{12}}b^{\frac{1}{3}},$$

$$C_0 = 0, \quad C_1 = \partial(u_0\,\partial u_0/\partial\xi + w_0\,\partial u_0/\partial\zeta)/\partial\zeta.$$

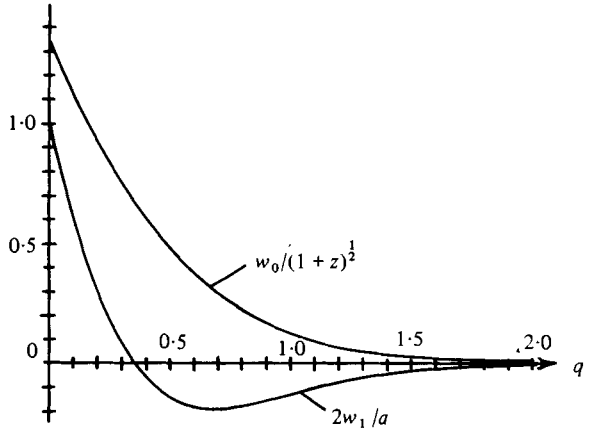

FIGURE 3. Transverse velocity for the free shear layer for stages 1, 2 and 3, where $w = E^{-\frac{1}{4}}b^{\frac{1}{2}}w_0 + RE^{-1}bw_1$, and $q = 2^{-\frac{3}{2}}E^{-\frac{1}{4}}b^{\frac{1}{2}}x(1+z)^{-\frac{1}{2}}$.

It turns out that this is the largest ϵ for this stage, so that the small-inertia restriction is $R \ll E^{\frac{11}{12}}b^{-\frac{1}{6}}$ for stage 1. The boundary conditions (5) now give

$$\partial^4\phi_i/\partial\zeta^4 + a^{-1}\,\partial\phi_i/\partial\zeta = C_i.$$

The boundary conditions

$$\phi_0 \to 1 - D(\xi), \quad \phi_1 \to 0 \quad \text{as} \quad \zeta \to -\infty, \tag{9a, b}$$

$$\phi_0 = 1, \quad \phi_1 = 0, \quad \partial\phi_i/\partial\zeta = 0 \quad \text{at} \quad \zeta = 0 \tag{9c, d, e}$$

come from matching the free shear layer and boundary conditions (6) at $z = 1$, respectively, where

$$D/2 = 1 - (1+2q^2)B_1 + 2qB_2, \quad q = 2^{-\frac{1}{2}}\xi,$$

which come from the free shear layer solution, evaluated at $z = 1$.

The solution of the ordinary differential equation governing ϕ_0 is

$$\phi_0 = 1 - D + DF_1(F_2 - F_3), \tag{10a}$$

where

$$F_1 = \exp(r), \quad F_2 = \cos(3^{\frac{1}{2}}r), \tag{10b, c}$$

$$F_3 = 3^{-\frac{1}{2}}\sin(3^{\frac{1}{2}}r), \quad r = \tfrac{1}{2}a^{-\frac{1}{3}}\zeta. \tag{10d, e}$$

Equations (8a) and (7b) now give u_0 and w_0, which, through C_1, give the inhomogeneous term in the ordinary differential equation governing ϕ_1. Again, particular and homogeneous solutions are combined to take care of both the inhomogeneous term and the boundary conditions; the result is

$$\phi_1 = \tfrac{1}{6}a^{\frac{1}{3}}DD'F_1[3F_1 + (4r-3)F_2 - (4r+7)F_3],$$

where $D' = dD/d\xi$. The functions $a^{\frac{1}{3}}u_0/D$ and u_1/DD' are universal profile functions of r only, but plots of these functions are not presented here.

For the intersection region and for stage 2, equations (2) give equations (7b, 8a), and

$$v_i = -y\,\partial^4\phi_i/\partial\zeta^4 + y\alpha^{\frac{1}{2}}C_i,$$

where

$$\zeta = E^{-\frac{1}{4}}(z-1), \quad \epsilon = RE^{-\frac{7}{8}}.$$

Again, this is the largest ϵ, so that the small-inertia restriction is $R \ll E^{\frac{7}{8}}$ for stage 2. The boundary conditions (5) now give the ordinary differential equations

$$a\,\partial^4\phi_i/\partial\zeta^4 - 2^{-\frac{1}{2}}\,\partial^2\phi_i/\partial\zeta^2 + \alpha\,\partial\phi_i/\partial\zeta = a\alpha^{\frac{1}{4}}C_i.$$

The boundary conditions (9) still hold.

The solutions depend upon the relationship between α and $\alpha_0 = (2^{\frac{1}{2}}/27a)^{\frac{1}{2}}$. For $\alpha > \alpha_0$,

$$\phi_0 = 1 - D + DG_1(G_2 - s_1 G_3/s_2), \tag{11a}$$

where

$$G_1 = \exp(s_1\zeta), \quad G_2 = \cos(s_2\zeta), \quad G_3 = \sin(s_2\zeta), \tag{11b, c, d}$$

$$s_1 = s_+ + s_-, \quad s_2 = 3^{\frac{1}{2}}(s_+ - s_-), \tag{11e, f}$$

$$s_\pm = 2^{-\frac{1}{2}}a^{-\frac{1}{2}}[\alpha \pm (\alpha^2 - \alpha_0^2)^{\frac{1}{2}}]^{\frac{1}{2}}. \tag{11g}$$

For $\alpha < \alpha_0$,

$$\phi_0 = 1 - D + D(t_+H_- - t_-H_+)/(t_+ - t_-), \tag{12a}$$

where

$$t_\pm = 2^{\frac{1}{2}}(3a)^{-\frac{1}{2}}\cos[\tfrac{1}{3}(\theta \pm 2\pi)], \tag{12b}$$

$$H_\pm = \exp(t_\pm\zeta), \quad \theta = 3\pi - \arccos(\alpha/\alpha_0). \tag{12c, d}$$

Equation (8a) now gives u_0. For $\alpha > \alpha_0$, u_0 is proportional to G_1G_3, so that the flow is alternately in the $\pm x$ direction between the planes $\zeta = k\pi/s_2$ for $k = 1, 2, 3, \ldots$; this is also true for both the intersection region and side layer for stage 1. For $\alpha < \alpha_0$, u_0 is proportional to $(H_- - H_+)$, so that the flow is in the $+x$ direction for all ζ; this is also true for both the intersection region and side layer for stage 3.

Equation (7b) now gives w_0, which, together with u_0, determines the inhomogeneous term in the equation governing ϕ_1. Again, particular and homogeneous solutions are combined to take care of both the inhomogeneous term and the boundary conditions (9b, d, e). For $\alpha > \alpha_0$,

$$\phi_1 = \tfrac{1}{12}\alpha^{\frac{1}{2}}DD'G_1[3G_1/s_1 + (4\zeta + s_3\zeta/as_2 - 3/s_1)\,G_2 - (6\alpha s_3\zeta + 7/s_2 + s_3/as_2^2)\,G_3],$$

where

$$s_3 = 2(\alpha^2 - \alpha_0^2)^{-\frac{1}{2}}/3^{\frac{3}{2}}.$$

For $\alpha < \alpha_0$,

$$\phi_1 = \alpha^{\frac{1}{4}}DD'[I_1H_+H_- + (J_+\zeta + K_+)\,H_- + (J_-\zeta + K_-)\,H_+],$$

where

$$J_\pm = \tfrac{1}{9}[1 + (2^{\frac{1}{2}}t_\pm \pm 2I_2)/(3\alpha - 2^{\frac{1}{2}}t_\mp \pm I_2)],$$

$$K_\pm = \pm(J_+ + J_- + I_1t_\mp)/(t_+ - t_-),$$

$$I_1 = \tfrac{1}{2}(t_+ + t_-)^{-1}, \quad I_2 = 3^{\frac{1}{2}}(\alpha_0^2 - \alpha^2)^{\frac{1}{2}}.$$

The velocities u_0 and u_1 cannot be rescaled into universal profile functions for stage 2. The profile functions u_0/D and u_1/DD' are functions of ζ and involve two independent parameters α and a.

For the intersection region and for stage 3, equations (2) give equations (7b, 8a) and $v_i = yC_i$, where now

$$\zeta = E^{-\frac{1}{4}}b(z-1), \quad \epsilon = RE^{-\frac{1}{4}}b^{\frac{3}{2}}.$$

Again, this is the largest ϵ, so that the small-inertia restriction is $R \ll E^{\frac{5}{4}}b^{-\frac{3}{2}}$ for stage 3. The boundary conditions (5) now give the ordinary differential equations

$$2^{-\frac{1}{2}}\partial^2\phi_i/\partial\zeta^2 - \partial\phi_i/\partial\zeta = -aC_i.$$

The side layer is separated from the $E^{\frac{1}{3}}$ layer at $z = 1$ by an $E^{\frac{1}{4}}$ layer, which matches the non-zero values of u_i in the side layer at $\zeta = 0$ and satisfies the boundary conditions (6), provided $w_i = 0$ in the side layer at $\zeta = 0$. Thus, the boundary conditions on ϕ_i are conditions (9*a*, *b*, *c*, *d*), while the no-slip conditions (9*e*) are relaxed.

Following the same procedure, we obtain

$$\phi_0 = 1 - D + DP, \quad \phi_1 = -2aDD'pP,$$

where $P = \exp(p)$, and $p = 2^{\frac{1}{2}}\zeta$. The functions

$$u_0/D = 2^{\frac{1}{2}}P, \quad u_1/aDD' = -2^{\frac{3}{2}}(1+p)P$$

are universal-profile functions of p alone. The inertialess velocity u_0 is positive for all ζ, while u_1 is negative for $0 > \zeta > -0{\cdot}707$ and positive for $\zeta < -0{\cdot}707$.

4. Side layer

Calderon & Walker (1977) present the inertialess solutions, ϕ_0, u_0, v_0 and w_0, for the side layer for each of the first three stages, and only the inertial perturbations, ϕ_1, u_1, v_1 and w_1, are presented here. The definition of ζ for the side layer for each stage is the same as that given in § 3 for the intersection region for the same stage.

For stage 1, equations (2) give

$$u_1 = \partial\phi_1/\partial\zeta, \quad v_1 = -y\,\partial^4\phi_1/\partial\zeta^4 + y\,\partial L/\partial\zeta, \tag{13a, b}$$

$$w_1 = \partial^3\phi_1/\partial\zeta^3 - \partial\phi_1/\partial X - L, \quad \epsilon = RE^{-\frac{3}{4}}b^{\frac{3}{2}}, \tag{13c, d}$$

where

$$L = u_0\,\partial u_0/\partial X + w_0\,\partial u_0/\partial\zeta, \quad X = bx. \tag{13e, f}$$

The boundary conditions (5) now give an ordinary differential equation governing ϕ_1,

$$\partial^4\phi_1/\partial\zeta^4 + (a+X)^{-1}\partial\phi_1/\partial\zeta = \partial L/\partial\zeta.$$

Since the total flow required by the condition (3) is taken care of by u_0, the net flow due to u_1 must be zero. In addition, the solution must satisfy the conditions (6) and (9*b*). The inhomogeneous term is determined from the solutions of Calderon & Walker (1977). Combining particular and homogeneous solutions to take care of the inhomogeneous term and these conditions, we obtain

$$\phi_1 = \tfrac{1}{7}a^2(a+X)^{-\frac{8}{3}}f_1[f_2 + f_3 - \tfrac{1}{5}f_1(4f_2^2 + 5)],$$

where

$$f_1 = \exp(\rho), \quad f_2 = \cos(3^{\frac{1}{2}}\rho),$$

$$f_3 = 3^{-\frac{1}{2}}\sin(3^{\frac{1}{2}}\rho), \quad \rho = \tfrac{1}{2}(a+X)^{-\frac{1}{3}}\zeta.$$

The rescaled axial velocities

$$U_0 = (a+X)^{\frac{4}{3}}u_0/4a = -f_1f_3,$$

$$U_1 = 7(a+X)^3u_1/16a^2 = f_1[f_2 - f_3 - f_1 + \tfrac{4}{3}f_1f_3(f_2+f_3)]$$

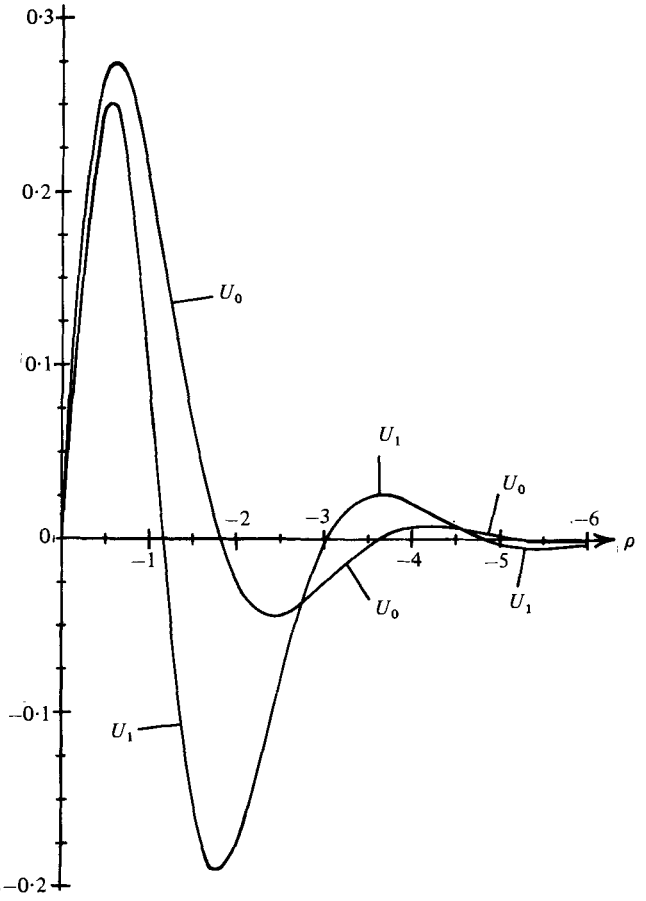

FIGURE 4. Axial velocity for the side layer for stage 1, where the inertialess velocity U_0, the inertial perturbation velocity U_1 and the boundary layer co-ordinate ρ have been rescaled.

depend only on ρ, and these universal velccity profile functions are plotted in figure 4. The inertialess flow consists of a strong forward jet adjacent to the wall

$$(-1{\cdot}81 < \rho < 0),$$

a weak backward jet beyond the wall jet ($-3{\cdot}63 < \rho < -1{\cdot}81$), and a very weak forward jet adjacent to the stagnant core ($-5{\cdot}44 < \rho < -3{\cdot}63$). The inertial perturbation velocity resembles the inertialess velocity, except that the corresponding zeros are closer to the wall. The perturbation velocity U_1 reaches its minimum value of $-0{\cdot}19$ at approximately $\rho = -1{\cdot}8$ where $U_0 = 0$, while U_1 reaches a local maximum of 0·026 at approximately $\rho = -3{\cdot}6$ where again $U_0 = 0$. The addition of small inertial effects to the inertialess flow increases the forward velocity near the wall, moves the zeros in the axial velocity toward the wall and increases the maximum magnitude of the velocity gradient.

For stage 2, equations (2) again give equations (13a, b, c, e), where now $\epsilon = RE^{-\frac{1}{2}}$ and $X = E^{\frac{1}{2}}x$. The inertial perturbations in the side layer and in the Ekman layers at $y = \pm(a+\alpha X)$ are comparable, so that the conditions (5) do not hold for this case. Equations (1) are written in two rescaled, right-handed Cartesian co-ordinate systems,

N, ζ, T, one system for the top and the other for the bottom. The N co-ordinate is measured perpendicular to the wall, into the fluid, and is stretched by $E^{-\frac{1}{2}}$; ζ is the same as the side-layer ζ; the T co-ordinate is measured along the wall in the $\mp x$ direction on the top and bottom, respectively, and is compressed by $E^{\frac{1}{4}}$. In the Ekman layers, w_0 and v_{T0} are $O(E^{-\frac{1}{4}})$, while v_{N0} and ϕ_0 are $O(1)$. The N component of equation (1*b*) indicates that ϕ_1 is independent of N and is therefore given by values in the side layer. The ζ and T components of equation (1*b*) give

$$\partial^2 w_1/\partial N^2 \mp v_{T1} = \partial\phi_1/\partial\zeta + v_{N0}\,\partial w_0/\partial N + w_0\,\partial w_0/\partial\zeta,$$

$$\partial^2 v_{T1}/\partial N^2 \pm w_1 = v_{N0}\,\partial v_{T0}/\partial N + w_0\,\partial v_{T0}/\partial\zeta,$$

where v_{N0}, w_0 and v_{T0} are obtained from the well-known inertialess Ekman layer solution (Howard 1969, p. 62). The boundary conditions are

$$w_1 = v_{T1} = 0 \quad \text{at} \quad N = 0,$$

$$w_1 \to 0, \quad v_{T1} \to \mp u_1 \quad \text{as} \quad N \to \infty.$$

Solutions are found by combining particular and homogeneous solutions, but are not presented here. Equation (1*a*) now gives an expression for $\partial v_{N1}/\partial N$. We integrate this expression from $N = 0$, where $v_{N1} = 0$, to $N = \infty$, to obtain modified Ekman conditions for the side-layer variables,

$$2^{\frac{1}{2}}\alpha u_1 \mp 2^{\frac{1}{2}} v_1 = \partial u_1/\partial\zeta - 0{\cdot}35\,\partial(u_0\,\partial u_0/\partial\zeta)/\partial\zeta \quad \text{at} \quad y = \pm(a+\alpha X).$$

The modified Ekman conditions and the solutions (13*a*, *b*, *c*, *e*) give an ordinary differential equation governing ϕ_1,

$$(a+\alpha X)\,\partial^4\phi_1/\partial\zeta^4 - 2^{-\frac{1}{2}}\,\partial^2\phi_1/\partial\zeta^2 + \alpha\,\partial\phi_1/\partial\zeta = (a+\alpha X)\,\partial L/\partial\zeta - 0{\cdot}35(2)^{-\frac{1}{2}}\,\partial(u_0\,\partial u_0/\partial\zeta)/\partial\zeta.$$

The solution must satisfy conditions (6) and (9*b*), and the net flow owing to u_1 must be zero. The inertialess solutions (Calderon & Walker 1977) and the inertial perturbations are different for $X \gtrless X_0 = a(\alpha_0^2 - \alpha^2)/\alpha$. The inertialess solutions are similar to those in the intersection region for stage 2, except that $s_\pm$ and $t_\pm$ in equations (11) and (12) are now functions of X, rather than constants. As a result, the term $\partial u_0/\partial X$ in L makes the inhomogeneous term in the equation governing ϕ_1 quite complex. The rather long and complicated solutions for ϕ_1 for various relationships between X and X_0 and between α and α_0 are not presented here, but are presented in El-Consul's thesis (1978, pp. 119–123).

For stage 3, equations (2) again give equations (13*a*, *b*, *c*, *e*, *f*), where now

$$\epsilon = RE^{-1}b^2.$$

However, when the inertialess solution (Calderon & Walker 1977) is introduced into equation (13*e*), we find that $L = 0$. Therefore, there is no inertial perturbation due to L, and ϵ is smaller than $RE^{-1}b^2$. The first non-zero inertial perturbation in the side layer is due to $u_0\,\partial w_0/\partial X + w_0\,\partial w_0/\partial\zeta$ and gives $\epsilon = Rb^2$. It turns out that the inertia perturbation in the $E^{\frac{1}{4}}$ layer, separating the side layer from the $E^{\frac{1}{3}}$ layer at $z = 1$, is much larger than that in the side layer. Since we are interested in the largest perturbation in the flow-carrying or adjacent regions for each stage, we will treat the $E^{\frac{1}{4}}$ layer, rather than the side layer, for stage 3.

Since Calderon & Walker (1977) only present inertialess solutions for flow-carrying regions, both inertialess solutions and inertial perturbations are presented here. For the $E^{\frac{1}{4}}$ layer at $z = 1$ and for stage 3, the orders of magnitude of the inertialess u, v and w are $E^{-\frac{1}{4}}b$, $E^{-\frac{1}{4}}b$ and b, respectively, while

$$\phi = 2a(a+X)^{-1} - 1 + E^{-\frac{1}{4}}b(\phi_0 + \epsilon\phi_1),$$

where $X = bx$, again. The equations (2) give

$$u_i = \partial\phi_i/\partial\eta, \quad v_i = -y\,\partial^4\phi_i/\partial\eta^4 + y\,\partial Q_i/\partial\eta, \tag{14a, b}$$

$$w_i = W_i + \partial^3\phi_i/\partial\eta^3 - Q_i, \quad \epsilon = RE^{-\frac{3}{4}}b, \tag{14c, d}$$

where

$$W_0 = 2a/(a+X)^2, \quad W_1 = Q_0 = 0, \tag{14e, f, g}$$

$$Q_1 = w_0\,\partial u_0/\partial\eta, \quad \eta = E^{-\frac{1}{4}}(z-1). \tag{14h, i}$$

The solutions must match the side-layer solutions, i.e.

$$u_i \to 2^{\frac{1}{2}}(a+X)\,W_i, \quad w_i \to W_i \quad \text{as} \quad \eta \to -\infty,$$

and must satisfy the boundary conditions (6) at $\eta = 0$.

The Ekman conditions (5) hold for the inertialess solution, so that the ordinary differential equation governing ϕ_0 is

$$2^{\frac{1}{2}}(a+X)\,\partial^4\phi_0/\partial\eta^4 - \partial^2\phi_0/\partial\eta^2 = 0.$$

The solution which satisfies the boundary conditions on the inertialess variables is

$$\phi_0 = \Phi_0 + 2^{\frac{7}{4}}a(a+X)^{-\frac{1}{2}}(m-M),$$

where

$$M = \exp(m), \quad m = \eta/2^{\frac{1}{4}}(a+X)^{\frac{1}{2}},$$

and Φ_0 is the $O(E^{-\frac{1}{4}}b)\,\phi$ in the side layer, evaluated at $\zeta = 0$, and is a function of X alone.

The inertial perturbations in the $E^{\frac{1}{4}}$ layer at $z = 1$ and in the adjacent Ekman layers at $y = \pm(a+X)$ are comparable, so that the conditions (5) do not hold for the inertial perturbation in the $E^{\frac{1}{4}}$ layer. The derivation of modified Ekman conditions parallels that for the side layer for stage 2. Now, η replaces ζ, T is compressed by b, v_{T0} and w_0 are $O(E^{-\frac{1}{4}}b)$, and v_{N0} and ϕ_0 are $O(E^{-\frac{1}{4}}b)$. When written in terms of u_0 and u_1 in the $E^{\frac{1}{4}}$ layer, evaluated at $y = \pm(a+X)$, the inertialess solutions and inertial perturbations in the Ekman layers are identical to those for stage 2. The modified Ekman conditions are now

$$\mp 2^{\frac{1}{2}}v_1 = \partial u_1/\partial\eta - 0{\cdot}35\,\partial(u_0\,\partial u_0/\partial\eta)/\partial\eta \quad \text{at} \quad y = \pm(a+X).$$

These conditions and equations (14*a*, *b*, *c*) give the equation governing ϕ_1,

$$2^{\frac{1}{2}}(a+X)\,\partial^4\phi_1/\partial\eta^4 - \partial^2\phi_1/\partial\eta^2 = 2^{\frac{1}{2}}(a+X)\,\partial Q_1/\partial\eta - 0{\cdot}35\,\partial(u_0\,\partial u_0/\partial\eta)/\partial\eta.$$

When the inertialess solution is introduced into the right-hand side of this equation, it turns out that the second term equals 0·35 times the first, so that the only effect of the Ekman-layer inertial perturbations is to reduce the $E^{\frac{1}{4}}$ layer inertial perturbation

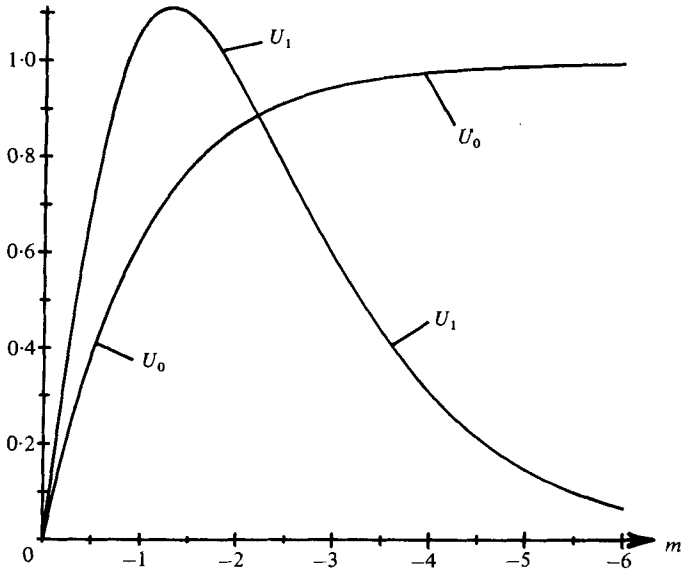

FIGURE 5. Axial velocity for the $E^{\frac{1}{4}}$ layer between the side layer and the wall at $z = 1$ for stage 3, and for the $E^{\frac{1}{4}}$ layers between the far core and the sides at $z = \pm 1$ for stage 4. The inertialess velocity U_0, the inertial perturbation velocity U_1 and the boundary layer co-ordinate m have been rescaled by different factors for stages 3 and 4.

by a factor of 0·65. Particular and homogeneous solutions are combined to take care of both the inhomogeneous term and the boundary conditions. The result is

$$\phi_1 = \Phi_1 + 2{\cdot}6a^2M(M+1-3m)/3(a+X)^2,$$

where Φ_1 is the $O(RE^{-\frac{1}{2}}b^2)\,\phi$ in the side layer, evaluated at $\zeta = 0$, and is a function of X alone. Since the side layer is inertialess to this order of magnitude, the $O(RE^{-\frac{1}{2}}b^2)$ side-layer solution is an inertialess solution with $u < 0$ for all ζ and with a negative total flow which exactly cancels the positive total flow due to u_1 in the $E^{\frac{1}{4}}$ layer, so that the total flow of $4a$ carried by u_0 in the side layer is not changed.

The rescaled axial velocities

$$U_0 = (a+X)\,u_0/2^{\frac{3}{4}}a = 1-M,$$

$$U_1 = 2^{\frac{1}{4}}(a+X)^{\frac{5}{2}}u_1/0{\cdot}52a^2 = \tfrac{10}{3}M(M-1-\tfrac{3}{2}m),$$

depend only on m, and these universal velocity profile functions are plotted in figure 5. The factor of 10 is included in the definition of U_1 so that U_0 and U_1 can be plotted with the same scale. The inertial perturbation increases the forward velocity throughout the $E^{\frac{1}{4}}$ layer and increases the velocity gradient near the wall ($-1{\cdot}6 < m < 0$).

5. Stage 4: $b = \mu E^{\frac{1}{2}}$

As $b \to O(E^{\frac{1}{2}})$, the thickness of the free shear layer $\delta_f \to O(1)$, and this layer evolves into the near core with all $O(1)$ derivatives. Calderon & Walker (1977) present the second-order, elliptic partial differential equation and boundary conditions governing

$\phi_0(x,z)$, and Calderon (1976) presents separation-of-variable solutions for this boundary value problem.

For the near core, equations (2) give

$$u_1 = \partial\phi_1/\partial z, \quad v_1 = yS,$$

$$w_1 = -\partial\phi_1/\partial x, \quad \epsilon = RE^{-\frac{1}{4}},$$

where

$$S = \partial(u_0\,\partial u_0/\partial x + w_0\,\partial u_0/\partial z)/\partial z - \partial(u_0\,\partial w_0/\partial x + w_0\,\partial w_0/\partial z)/\partial x.$$

This is the largest ϵ for this stage, so the small-inertia restriction is $R \ll E^{\frac{1}{4}}$ for stage 4. The Ekman conditions (5) give the equation governing ϕ_1,

$$\partial^2\phi_1/\partial x^2 + \partial^2\phi_1/\partial z^2 - 2^{\frac{1}{2}}\mu\,\partial\phi_1/\partial z = -2^{\frac{1}{2}}aS.$$

Since the inertial perturbations in adjacent subregions are much smaller than that in the near core, the boundary conditions are

$$\phi_1 = 0 \quad \text{at} \quad z = \pm 1 \quad \text{and at} \quad x = 0,$$

$$\phi_1 \to 0 \quad \text{as} \quad x \to \infty.$$

When the inertialess variables (Calderon & Walker 1977) are introduced into the expression for S, it becomes

$$S = 2^{\frac{1}{2}}\mu((\partial\phi_0/\partial z)\,\partial^2\phi_0/\partial x\,\partial z - (\partial\phi_0/\partial x)\,\partial^2\phi_0/\partial z^2),$$

where ϕ_0 is given by the sum of separation-of-variable solutions (Calderon 1976). The inhomogeneous term in the equation governing ϕ_1 involves products of infinite series, and it appears that a numerical analysis, such as a relaxation scheme, would be required to solve for ϕ_1. Such a numerical analysis has not been carried out.

As $b \to O(E^{\frac{1}{4}})$, the thickness of the side layer for stage 3, $\delta_s \to O(1)$, and this layer evolves into the far core. When we introduce the inertialess solution for the far core (Calderon & Walker 1977) into equations (2), we find that the leading inertia term

$$u_0\,\partial u_0/\partial X + w_0\,\partial u_0/\partial z = 0,$$

where $X = E^{\frac{1}{4}}x$ for stage 4. The first non-zero inertia term gives $\epsilon = RE$. It turns out that the inertial perturbations in the $E^{\frac{1}{4}}$ layers at $z = \pm 1$ are much larger than that in the far core. Therefore, we treat only the inertial perturbations in the $E^{\frac{1}{4}}$ layers that separate the far core from the $E^{\frac{1}{4}}$ layers at $z = \pm 1$.

In the $E^{\frac{1}{4}}$ layers, the orders of magnitude of the inertialess u, v and w are 1, $E^{\frac{1}{4}}$ and $E^{\frac{1}{2}}$, respectively, while

$$\phi = g - \coth(e) + E^{\frac{1}{4}}(\phi_0 + \epsilon\phi_1),$$

where

$$e = 2^{\frac{1}{2}}\mu, \quad g = a(a+\mu X)^{-1}\,\mathrm{cosech}\,(e)\exp(\pm e)$$

for the layers at $z = \pm 1$. Equations (2) again give equations (14*a*, *b*, *c*, *f*, *g*, *h*), while equations (14*d*, *e*, *i*) are replaced by

$$\epsilon = RE^{-\frac{1}{4}}, \quad W_0 = \mu g/(a+\mu X),$$

$$\eta = E^{-\frac{1}{4}}(z \mp 1), \quad \text{at} \quad z = \pm 1,$$

respectively. Matching the far-core solution gives the boundary conditions

$$u_i \to 2^{\frac{1}{2}}(a+\mu X)\,W_i, \quad w_i \to W_i \quad \text{as} \quad \eta \to \mp\infty,$$

for the layers at $z = \pm 1$, while the solutions must also satisfy the boundary conditions (6) at $\eta = 0$. The analysis is the same as that given in § 4 for the $E^{\frac{1}{4}}$ layer at $z = 1$ for stage 3. The results are

$$\phi_0 = \Phi_0(X, \pm 1) \pm 2^{\frac{3}{2}}\mu g(a+\mu X)^{\frac{1}{2}}(m-M),$$

$$\phi_1 = \Phi_1(X, \pm 1) + 0{\cdot}65\mu^2 g^2 M(M+1-3m)/3,$$

for the layers at $z = \pm 1$, where now

$$m = \pm\eta/2^{\frac{1}{4}}(a+\mu X)^{\frac{1}{2}}, \quad M = \exp(m),$$

while $\Phi_0(X, z)$ and $\Phi_1(X, z)$ are the $O(E^{\frac{1}{4}})$ and $O(R)$ terms in the asymptotic expansion for ϕ in the far core.

The rescaled axial velocities in the $E^{\frac{1}{4}}$ layers at $z = \pm 1$

$$U_0 = u_0/2^{\frac{1}{2}}\mu g = 1 - M,$$

$$U_1 = \pm 2^{\frac{1}{4}}(a+\mu X)^{\frac{1}{2}}\,u_1/0{\cdot}13\mu^2 g^2 = \tfrac{10}{3}M(M-1-\tfrac{3}{2}m)$$

are the same universal velocity profile functions of m as those given in § 4 for the $E^{\frac{1}{4}}$ layer at $z = 1$ for stage 3 and plotted in figure 5. For the $E^{\frac{1}{4}}$ layer at $z = 1$, $U_1 > 0$ and the remarks given in the previous section apply here as well. However, for the $E^{\frac{1}{4}}$ layer at $z = -1$, $U_1 < 0$, so that the inertial perturbation velocity decreases the forward inertialess velocity throughout the layer and decreases the velocity gradient near the wall ($-1{\cdot}6 < m < 0$).

6. Concluding remarks

The present analysis is the beginning of a bridge between inertialess solutions for arbitrary geometry and inertial–viscous solutions for restricted geometry. At this point, direct comparison of the present solutions and any inertial–viscous solutions is not possible because the geometries are different. Walker (1975) showed that the solution for any variable-area, rectangular duct with symmetrically diverging or converging top and bottom or sides can be constructed from the solutions for the prototype considered here, so that the latter contain all of the significant phenomena in variable-area, rectangular duct flows. The objective here is to treat the prototype for all possible geometries, here represented by b, with the assurance that flows are similar in any variable-area, rectangular duct. Extensions are planned to cover inertial–viscous solutions in the prototype for various values of b and to cover inertial perturbations to inertialess flows past bumps or ridges with $h \gg E^{\frac{1}{4}}$ in constant-area, rectangular ducts.

The ratio of each inertial perturbation to the corresponding inertialess variable in the side layer, for stages 1 and 2, and in the $E^{\frac{1}{4}}$ layers, for stages 3 and 4, approaches zero, at least as fast as X^{-1}, as $X \to \infty$. Therefore, inertial effects do not accumulate over long duct lengths and do not become significant far downstream. Instead, the small inertial effects become even smaller far downstream.

The present solutions are for flows with diverging top and bottom. The solutions for flows with converging top and bottom are obtained from the present solutions by simply changing the direction of flow, i.e. by changing the right-hand side of equation (3) to $-4a$. The result is simply a change of sign for some variables, while others remain the same.

This research was supported partly by the National Science Foundation under Grant ENG-7423778 and partly by the University of Al-Fateh at Tripoli, Libya.

REFERENCES

BOYER, D. L. 1971 Rotating flow over a step. *J. Fluid Mech.* **50**, 675–687.

CALDERON, A. 1976 Steady flow in rapidly rotating rectangular ducts with small divergences. Ph.D. thesis, University of Illinois at Urbana-Champaign.

CALDERON, A. & WALKER, J. S. 1977 Steady flow in rapidly rotating variable-area rectangular ducts. Part 2. Small divergences. *J. Fluid Mech.* **81**, 353–368.

EL-CONSUL, A. M. 1978 Inertial perturbations to inertialess magnetohydrodynamic and rotating flows. Ph.D. thesis, University of Illinois at Urbana-Champaign.

FOSTER, M. R. 1975 Rotating flow past an elliptic-cylindrical bump of large aspect ratio. *Z. angew. Math. Phys.* **26**, 789–806.

GREENSPAN, H. P. 1968 *The Theory of Rotating Fluids.* Cambridge University Press.

HOWARD, L. N. 1969 *Rotating Flow.* Lectures at the Royal Institute of Technology, Stockholm.

HSEUH, Y. & LEGECKIS, R. 1973 Western intensification in a rotating water tunnel. *Geophys. Fluid Dyn.* **5**, 333–358.

HUPPERT, H. E. & STERN, M. E. 1974 The effect of side walls on homogeneous rotating flow over two-dimensional obstacles. *J. Fluid Mech.* **62**, 417–436.

JACOBS, S. J. 1964 The Taylor column problem. *J. Fluid Mech.* **20**, 581–591.

ROBERTS, P. H. 1967 *An Introduction to Magnetohydrodynamics.* Elsevier.

VAZIRI, A. & BOYER, D. L. 1971 Rotating flow over shallow topographies. *J. Fluid Mech.* **50**, 79–95.

WALKER, J. S. 1975 Steady flow in rapidly rotating variable-area rectangular ducts. *J. Fluid Mech.* **69**, 209–227.